A global historical ozone data set and prominent features of stratospheric variability prior to 1979

Stefan Brönnimann, Jonas Bhend, Jörg Franke, Simon Flückiger, Andreas Fischer, René Bleisch, Greg Bodeker, Birgit Hassler, Eugene Rozanov, Martin Schraner

Supplementary material

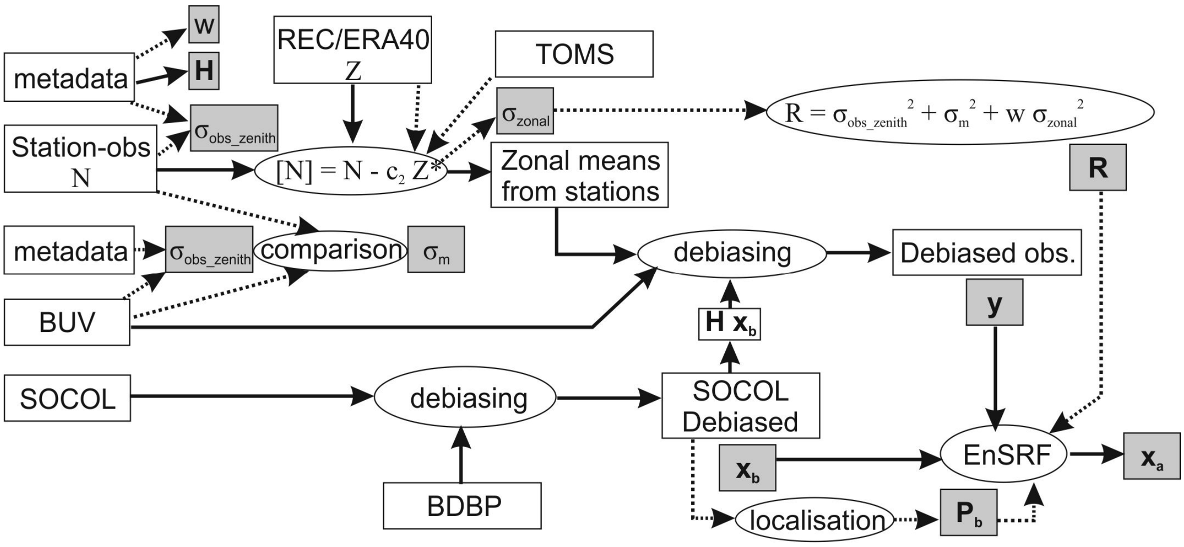

Figure S1. Schematic depiction of the approach.

Supplementary Section S4: Data processing and auxiliary steps

S4.1. Model assessment

As only total column ozone is assimilated, it is vital that the model simulates a realistic vertical distribution of ozone and its covariance structure. We therefore assessed the zonal mean ozone variability in the simulations and specifically the effect of external forcings (for further validation studies see SPARC CCMVal, 2010; Fischer et al., 2008b; Scaife et al., 2008).

A multiple linear regression model was applied to the ensemble mean. As our main focus was to reproduce the effects of dynamical and radiative processes in the northern winter polar stratosphere, the regression model was applied to zonally averaged variables over the winter months, *i.e.* January to March. The predictor variables, which were computed from the model boundary conditions, comprise two quasi-orthogonal QBO time series (zonal mean equatorial winds at 10 hPa and 30 hPa, the latter with a lag of 2 months), total solar irradiance, stratospheric aerosol optical depth in the layer between 15 and 35 km altitude, greenhouse gas concentrations, and equivalent effective stratospheric chlorine. From the SST fields, indices for El Niño (NINO3.4 index with one month lead time), the Pacific Decadal Oscillation (PDO, Mantua et al., 1997), and the Atlantic Multidecadal Oscillation (AMO, Enfield et al., 2001) were computer as additional predictor variables. The regression-based validation was applied to different simulated variables of SOCOL, but for brevity's sake we only discuss the outcome for ozone. The patterns of ozone changes associated with each of the regression model basis functions (predictor variables) are shown in Fig. S2.

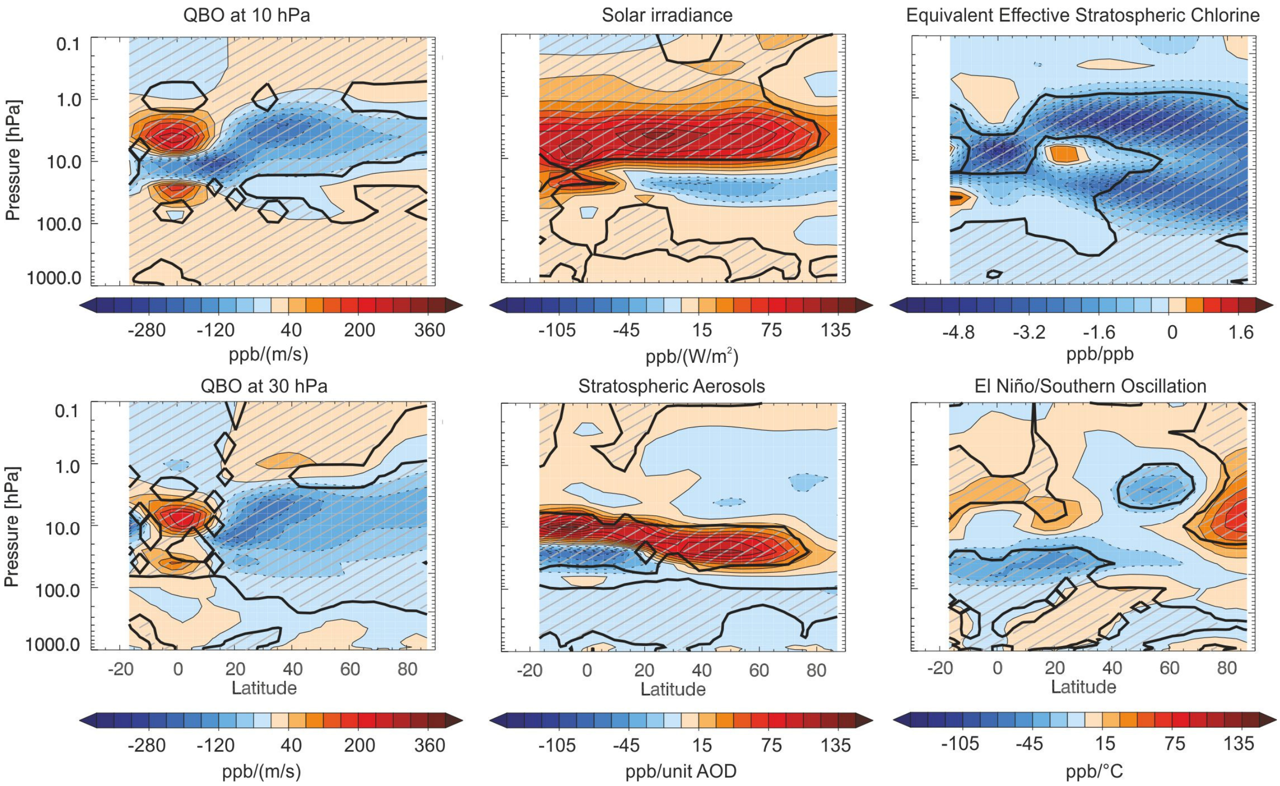

Figure S2. Coefficients of a multiple regression model with zonal mean ozone mixing ratios of the ensemble mean as predictand and various predictor variables. Shaded areas, together with black contour line, mark statistically significant areas (p-value < 0.05). For comparability reasons the regression-coefficients are displayed as ppbv change with respect to one standard deviation of the predictor. Due to the long-term trend in EESC, however, this coefficient is plotted with respect to 100 pptv.

The well-documented relation of ozone to the QBO (*e.g.,* Baldwin et al., 2001) with a dipole-structure over the equatorial stratosphere and decreases in ozone over the whole northern hemisphere is well captured in SOCOL. This is also the case for the response to solar variability that exhibits strong increases in ozone in the tropical upper stratosphere with an increase in solar activity, in line with Hood and Soukharev (2012). Regarding stratospheric aerosol loading, ozone shows a positive response to increased aerosols over much of the northern hemispheric stratosphere. While this may be surprising at first sight, this behaviour can be understood by the fact that the stratospheric aerosol facilitates heterogeneous activation of halogen containing species while suppressing the reactive nitrogen oxides. Therefore, different catalytic chemical cycles are dominant depending on the stratospheric burden of ozone depleting substances (Tie and Brasseur, 1995). This becomes relevant when studying the full 20th century with some large volcanic eruptions prior to the strong increase of anthropogenic halogens in the stratosphere. In this case ozone increase caused by the deactivation of reactive nitrogen can dominate. As expected, ozone shows a strong anti-correlation with effective stratospheric chlorine, over the whole northern hemisphere. Finally, the response to ENSO can be best described by a change in the strength of the Brewer-Dobson circulation (BDC) (e.g. Fischer et al., 2008a, see also Hood and Soukharev, 2012) that leads to an ozone decrease in the tropical lower stratosphere and strengthened transport of equatorial ozone towards to the North Pole.

These results show that the model captures well the effect of the boundary conditions on ozone. As a result, we expect skill relative to climatology from the boundary conditions alone (as already shown in Fischer et al. 2008), without yet incorporating observations. Moreover, due to the physical consistency, we expect the covariance matrices to capture physically and chemically relevant processes in a realistic manner. The data set is thus suitable for the chosen off-line data assimilation.

S4.2. Debiasing of model data

Ozone in SOCOL has a seasonally varying bias in its climatology relative to the BDBP validation data set. We removed the bias by means of a regression model that was fitted in the overlapping period 1979-1999 and applied to the preceding period (the bias consists of an ozone-invariant part and one part that is dependent on the modelled ozone amount). The results of this step are shown in Fig. 3 for two levels in three different zonally averaged regions. In general, the debiasing works well and brings the time series closer to the observations. There is, in general, good agreement with respect to the interannual variability (the agreement is solely due to boundary conditions). Yet, in some regions and levels, the trends and/or seasonality do not agree well.

S4.3. Adjustment of ground-based total ozone to zonal means

The ground based total column ozone data represent ozone at a given location, whereas the assimilation procedure requires zonal averages. Because station data are too sparse to form averages over latitude bands, the data from each station were adjusted to represent the zonal mean total ozone of the corresponding latitude. We assumed that the deviation of total ozone at a given location from its mean seasonal cycle has a large-scale, zonal mean contribution which arises, for instance, from changes in the BDC, and a zonally non-uniform change that results from an ozone redistribution in the lowermost stratosphere. To account for the latter, we assumed that the deviation N^* of total ozone from its zonal mean $[N]$ is related to the deviation Z^* of 200 hPa GPH from its zonal mean $[Z]$. Previous work has shown the strong relation between midlatitude total ozone and 200 hPa GPH (Brönnimann et al., 2000) in all seasons. For each calendar month, we fitted the regression model:

$$N = c_0 + c_1 [Z] + c_2 Z^* + \varepsilon, \qquad \text{(S1)}$$

from which $[N]$ can be estimated as $N - c_2 Z^*$. To test the approach, the algorithm was applied to TOMS total column ozone and ERA-40 200 hPa GPH data for the period 1979-2000. Figure S3 shows the results for two selected months, Feb. 1999 and Aug. 1980. Although the zonally asymmetric features are weakened (in some cases considerably), part of the zonal asymmetry remains. This remaining structure must be accounted for in the calculation of the observation error (see Sect. S4.5).

S4.4. Debiasing of total column ozone data

Recall that the model data were debiased with respect to BDBP in the overlapping period. A similar debiasing is necessary for the total column ozone observations (both ground-based and BUV satellite data). We applied H to the debiased model data $\overline{\mathbf{x}_b}$ and calculated the difference from observations, *i.e.,* $\mathbf{y} - H(\overline{\mathbf{x}_b})$ (BDBP could not be used instead of $\overline{\mathbf{x}_b}$ as many observation series do not overlap with BDBP). To this difference we fitted in each sequence (*i.e.,* each part of a series that was obtained with the same instrument type and observation mode, see Table S1) the first harmonic of the seasonal cycle using least squares regression and subtracted it from the observations.

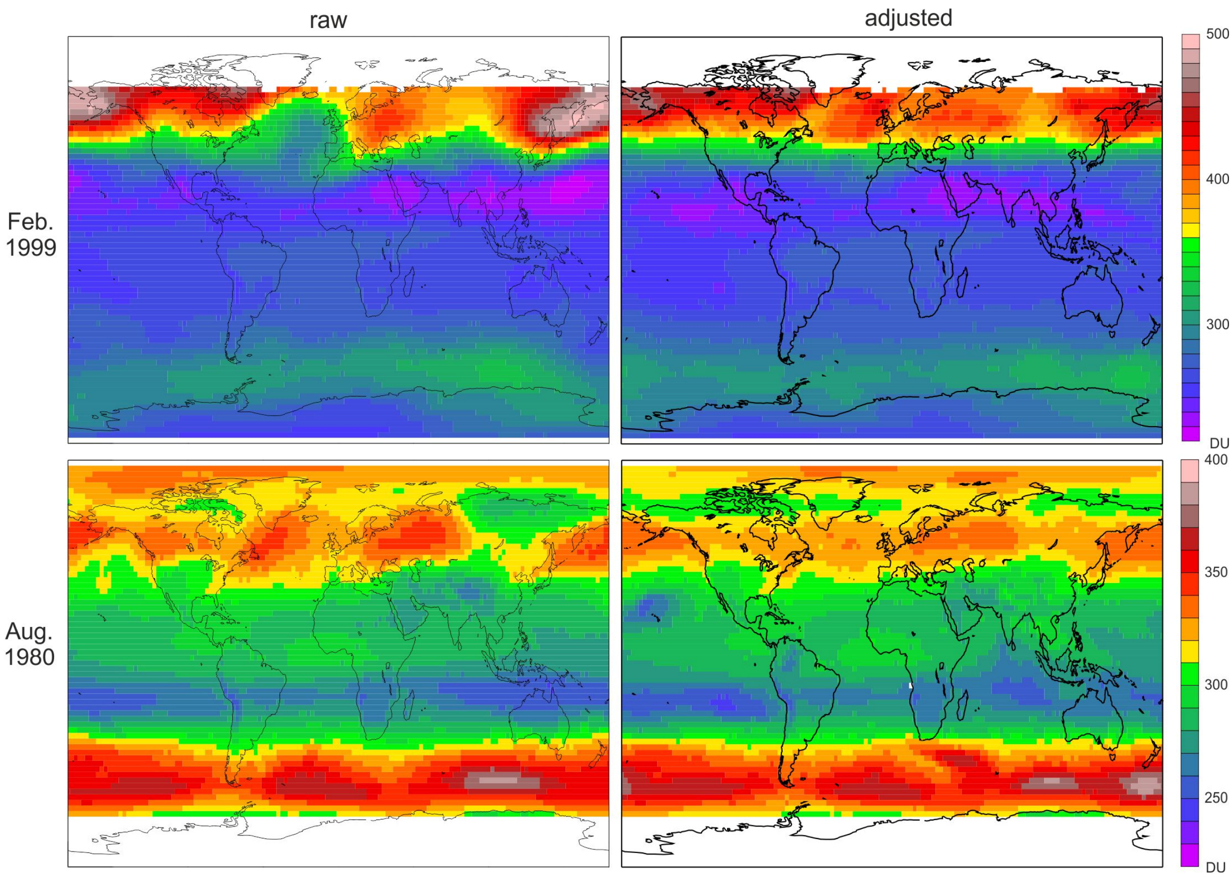

Figure S3. Comparison of raw and zonally adjusted TOMS total column ozone data for February 1999 and August 1980.

S4.5. Construction of observation error covariance matrix

R is a diagonal matrix that contains the observation error variances. We assume that the error variance consists of several sources of errors which can be quantified individually and which are independent from each other:

$$\sigma_{obs\_error}^2 = \sigma_{obs\_zenith}^2 + \sigma_m^2 + \sigma_{zonal}^2. \qquad \text{(S2)}$$

Here σ_{obs_zenith} is the error of a zenith observation, which is mainly an instrumental error, σ_m is the error that depends on the air mass and hence on the atmosphere, and σ_{zonal} is the error due to insufficient adjustment to zonal means. The error σ_{obs_zenith} is estimated from the corresponding literature (Tab. S1). For instance, the quality statements for "precision" in Brönnimann et al. (2003b) were translated in the following way: 4 DU for "excellent", 8 DU for "very good", 12 DU for "good" and 16 DU for "fair" (stations rated as "poor" were not considered at all). The Table Mountain data from the Smithsonian Institution received an error of 20 DU. We proceeded similarly for other series, attributing 4 DU to the homogenized long-term series and 6 DU to all other post-1957 data (see Table S1). This is broadly consistent with the literature (Mérgie, 1989; Brönnimann et al., 2003b), although most references do not specifically refer to monthly means.

Comparisons between BUV and ground-based total column ozone data were performed in the late 1970s and early 1980s, but focusing on the accuracy rather than the precision (Mérgie, 1989; WMO, 1980, 1983). Differences were found to lie in the range of 17 DU or larger than 3%.

For estimating σ_{obs_zenith} and σ_m for BUV we compared daily ground-based total column ozone data from Arosa and Oxford with BUV total column ozone data distance-weighted within a 4° x 4° square around these stations from the same day (R. Bleisch, unpublished report). A regression approach was performed incorporating a linear trend as well as dependencies on total ozone, air mass, and reflectivity (from BUV data) or cloud cover (estimated from ground based stations). Results showed that by far the most important contributor to the variations in differences is air mass. Additional but smaller influences were found for the trend and (in the case of Oxford) for total column ozone. The standard deviation of the (daily) residuals was between 10 and 15 DU. Based on these results we set σ_{obs_zenith} for monthly means to 10 DU for BUV data. Given our confidence in the Arosa series (Staehelin et al., 1998), we attribute most of the air mass dependent error to the BUV data and assume a 2% error per unit air mass for BUV and a 0.5% error for ground-based data (assuming local noon for all observations).

For determining σ_{zonal} we analysed the zonal standard deviation of the adjusted TOMS data (see Sect. S4.3). Smoothing the dependence on latitude and on the seasonal cycle resulted in an estimation of σ_{zonal} (Fig. S4). Note that up to this point observation errors were considered to be uncorrelated with each other. This is, however, not the case for σ_{zonal}, which is similar for two stations close to each other. Rather than letting **R** become non-diagonal, we accounted for this problem by multiplying σ_{zonal} for each station with a weight that depends on the distances D_i to all stations i, including the station itself. These distances were first transformed using an exponential function (see Eq. S1) with a length scale L of 1000 km (representing a typical decorrelation scale for upper-level variables, Griesser et al., 2010) and then summed over all stations in all latitude bands. Hence, **R** is then a diagonal matrix with r for each observation in the diagonal:

$$r = \sigma_{obs\_zenith}{}^2 + \sigma_m{}^2 + \sigma_{zonal}{}^2 \sum_i exp(\frac{-D_i{}^2}{2L^2}) \qquad \text{(S1)}$$

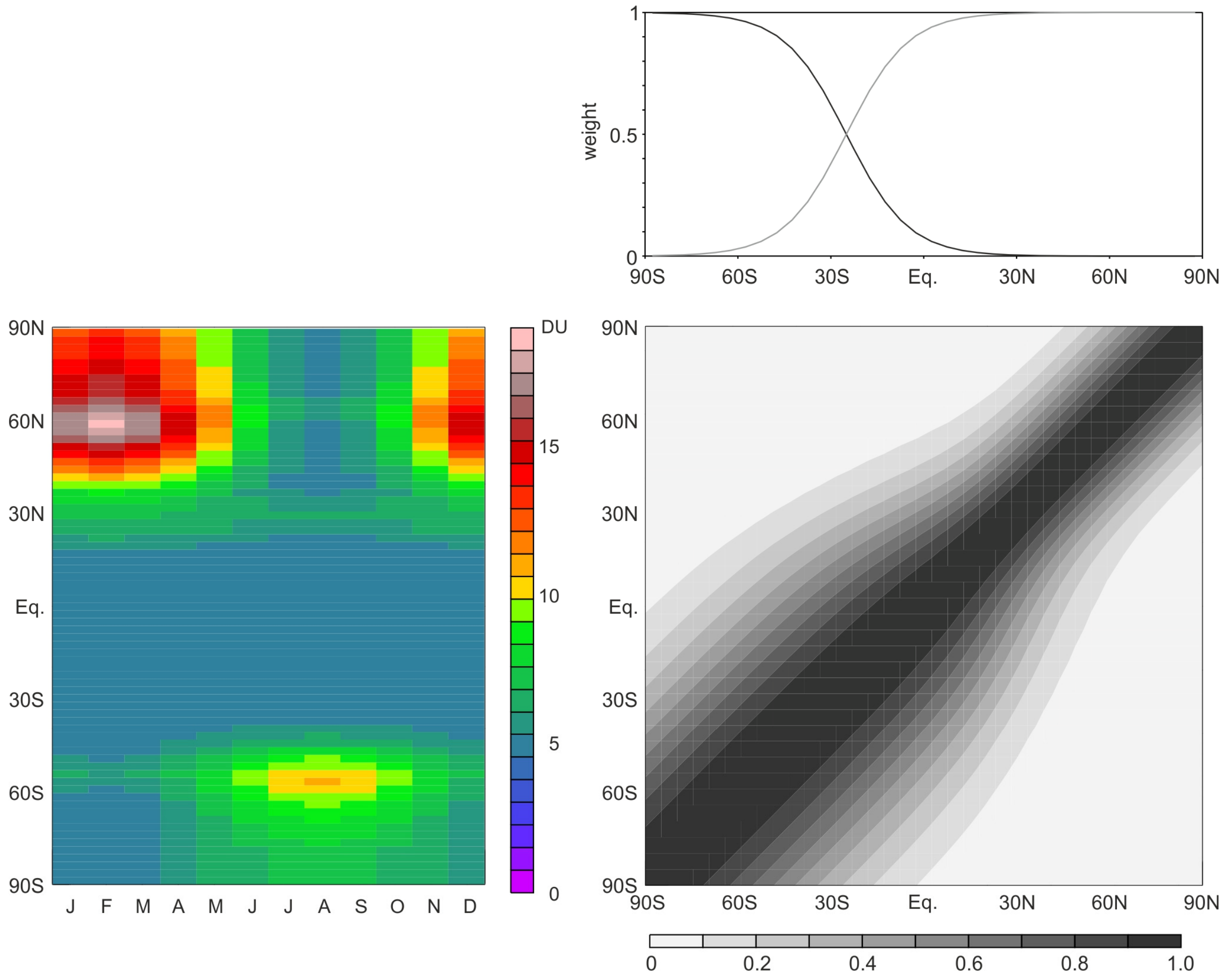

Figure S4. Left: Error of the zonal adjustment as a function of calendar month and latitude. Right: Localisation weights of the background error covariance matrix. The top panel shows the function *a* (grey is for boreal winter, black is for aural winter) used to determine the weights.

S4.6. Assessment of observation errors

The consistency of errors was assessed monthly by analysing the fraction of differences $|\mathbf{y} - \mathbf{H}\overline{\mathbf{x}_b}|$ larger than $2\sqrt{(\sigma_{obs\_error}^2 + \sigma_{ensemble}^2)}$ for the series in Fig. 4 (Rome, Nashville, Tateno, and corresponding BUV data). Assuming a Gaussian distribution of errors and no bias, a fraction of 5% is expected. We find fractions of 7%, 5%, 19%, and 8%, respectively. The high fraction for Tateno could be due to a remaining seasonally varying bias. The assimilation procedure requires that $|\mathbf{y}\text{-}H(\overline{\mathbf{x}_b})| < 3\sqrt{(\sigma_{obs\_error}^2+\sigma_{ensemble}^2)}$. As a consequence, the erroneous BUV data are not assimilated and the fractions are further reduced. Hence, our error estimates that are based on metadata and independent analyses are broadly consistent with the differences, but further improvements on the side of the observations (debiasing, homogenisation, outlier screening) might be beneficial.

S4.7. Background error covariance

The background covariance matrix $\mathbf{P^b}$ was estimated from the ensemble covariance matrix. Unfortunately, our ensemble is small (nine members). Spurious correlations may occur far off the diagonal which may affect the results. A localisation of the matrix (or similar adjustment) is therefore necessary. The covariance matrix was localised in latitude and time, leaving the altitude dimension unaltered. The localisation followed the principle of distance weighting as above (see also Bhend et al., 2012). Ozone is strongly affected by the BDC, which shows a distinct, seasonally dependent, latitudinal structure. Therefore the distance weighting was altered to allow long-range correlations during times and regions when the BDC is active. We accounted for this by weighting the distance with a function *a* in the following way:

$$w_{i,j} = \sqrt{a_i a_j}\exp\left(\frac{-D^2}{2L_1^2}\right) + \sqrt{(1-a_i)(1-a_j)}\exp\left(\frac{-D^2}{2L_2^2}\right) \qquad \text{(S2)}$$

Here, $w_{i,j}$ represent scaling factors applied to the covariances between elements i and j of $\mathbf{x_b}$. D in this case is the latitudinal distance (in degrees; L_1 is set to 20°, L_2 is set to 40°). The function *a* depends on the season, switching the sign of the latitude axis between boreal winter (Nov.-Apr.) and austral winter (May-Oct.). Function *a* and the resulting matrix of scaling factors are shown in Fig. S4. Localisation was also applied in time, setting L to 3 months (consistent with Fioletov and Shepherd, 2003).

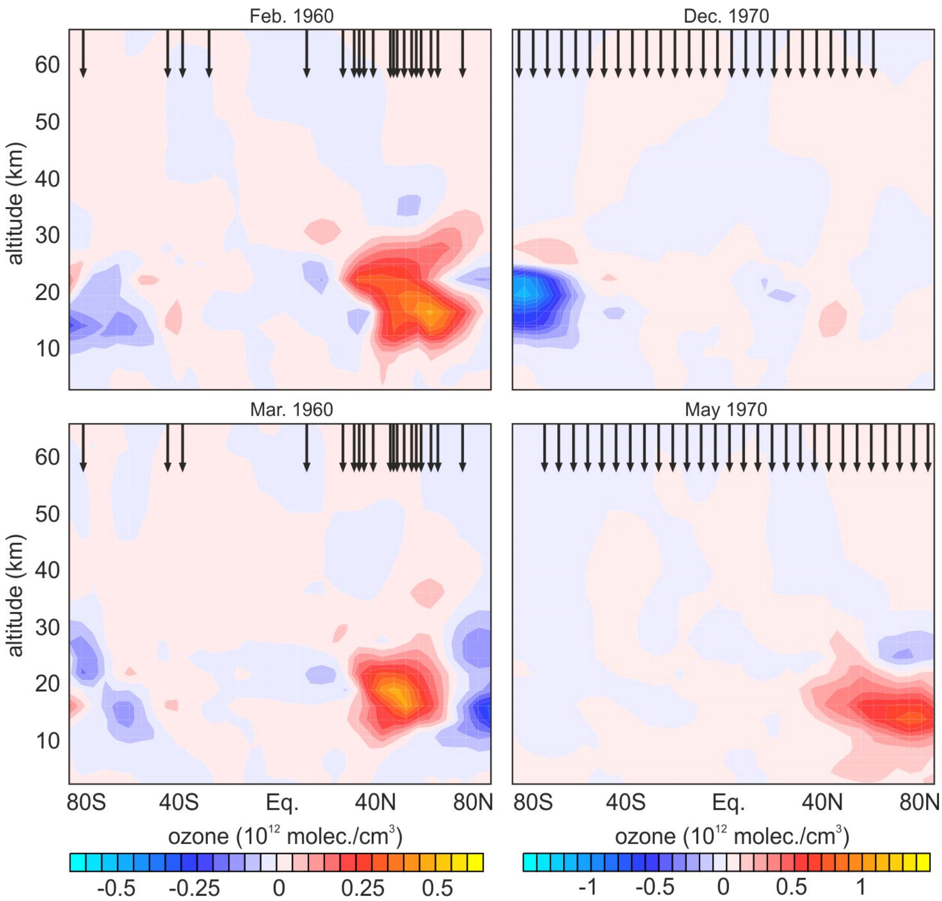

Figure S5. Results of the assimilation. Shown are the differences (assimilation minus background) for four sample months. Arrows indicate locations where observations (ground-based in the left two cases, BUV in the right two cases, note the different scale) were assimilated.

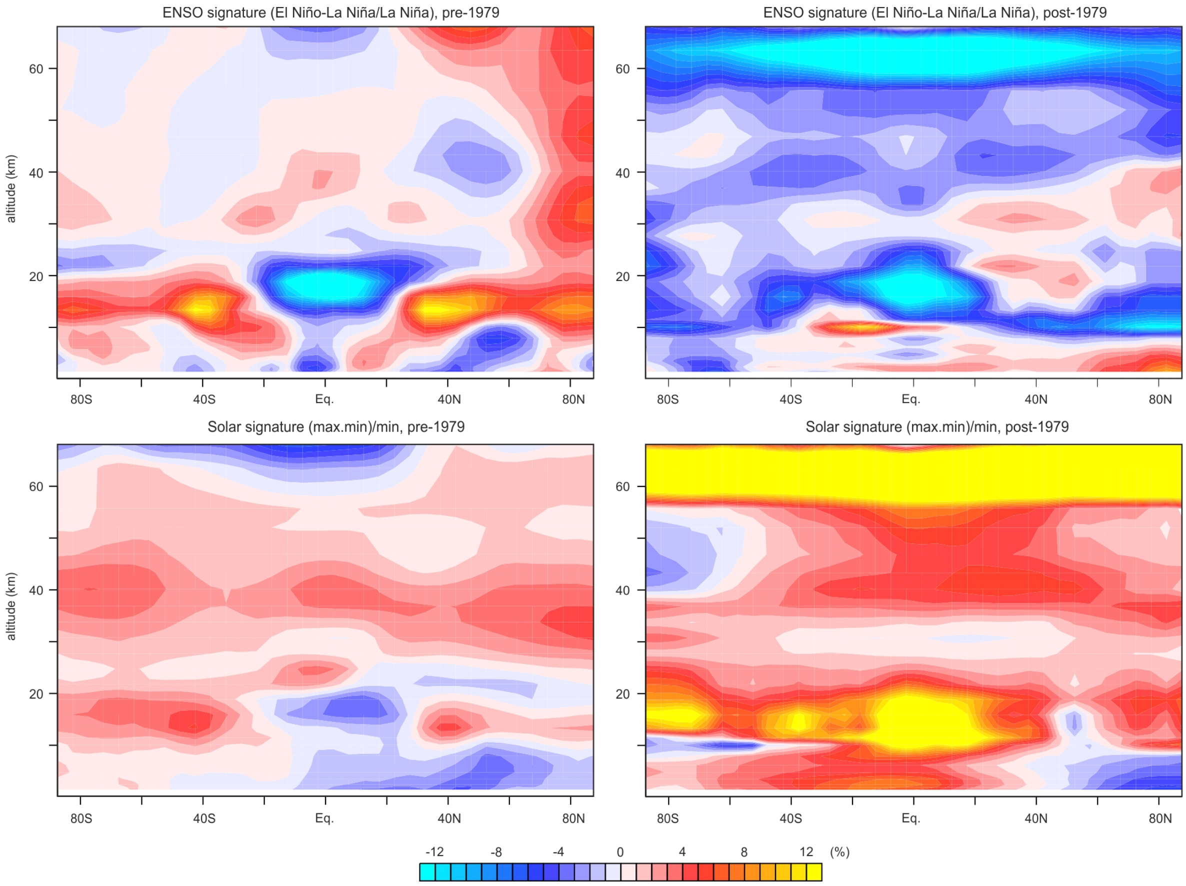

Figure S6. (top) Differences in ozone between El Niño and La Niña events in the pre-1979 period in HISTOZ (left) and the post-1979 period in BDBP. (bottom) Differences in ozone between solar maxima and solar minima in the pre-1979 period in HISTOZ (left) and the post-1979 period in BDBP. Note that the figures are the same as in Fig. 10 and 11, but plotted in terms of relative rather than absolute differences.

Table S1. List of stations with ground-based total ozone observatios used for the assimilation. Station start years in brackets denote changes in the instrument. Error 1 and 2 refer to the pre-1957 and post-1957 periods.

Station name	lon (°E)	lat (°N)	Start Year	n	Reference (pre-IGY only)	Source	error1	error2
Aarhus	10.6	56.3	1940 (1952)	227	Brönnimann et al. 2003ab	WOUDC	16	6
Aldergrove	-6.2	54.7	1952	54	Brönnimann et al. 2003ab	WOUDC	4	6
Alma-Ata	76.9	43.3	1974	58		WOUDC	8	6
Arosa	9.7	46.8	1926	588	Staehelin et al. 1998	WOUDC	4	4
Aspendale	145.1	-38.0	1957	256		WOUDC	8	6
Belsk	20.8	51.8	1963	185		WOUDC	8	6
Bismarck	-46.8	46.8	1957	216		WOUDC	8	6
Bombay	72.9	18.9	1936	17	Brönnimann et al. 2003ab	WOUDC	12	6
Brisbane	153.1	-27.4	1957	254		WOUDC	8	6
Buenos Aires	-58.5	-34.6	1965	156		WOUDC	8	6
Cairo	31.3	30.1	1928	135	Brönnimann et al. 2003ab	internal	8	6
Camborne	-5.3	50.2	1952	176	Brönnimann et al. 2003ab	WOUDC	12	6
Canberra	149.0	-35.3	1929	45	Brönnimann et al. 2003ab	internal	12	6
Caribou	-68.1	46.9	1958	199		WOUDC	8	6
Christchurch	172.6	-43.5	1928	116	Brönnimann et al. 2003ab	WOUDC	8	6
College	-147.5	64.7	1952	78	Brönnimann et al. 2003ab	WOUDC	16	6
Darwin	130.9	-12.4	1966	100		WOUDC	8	6
Dombas	9.1	62.1	1940	67	Svendby et al. 2003	WOUDC	8	6
Edmonton	-113.5	53.6	1950	282		WOUDC	8	6
Flagstaff	-111.7	35.2	1954	82		internal	8	6
HalleyBay	-26.7	-75.5	1957	94		WOUDC	8	6
Hemsby	1.7	52.7	1952	36	Brönnimann et al. 2003ab	WOUDC	8	6
Hobart	147.5	-42.8	1967 (1973)	120		WOUDC	8	6
Huancayo	-75.3	-12.0	1964	176		WOUDC	8	6
Kagoshima	130.5	31.7	1958	236		WOUDC	8	6
King Edward Point	-36.5	-54.2	1971	91		WOUDC	8	6
Kodaikanal	77.5	10.2	1928	245	Brönnimann et al. 2003ab	internal	8	6
Lerwick	-1.2	60.1	1926 (1952)	295	Brönnimann et al. 2003ab	internal	4	6
Magny	2.1	48.7	1955	75	Brönnimann et al. 2003ab	WOUDC	8	6
Marseille	5.4	43.3	1927	22	Brönnimann et al. 2003ab	internal	8	6
Mauna Loa	-155.6	19.5	8	203		WOUDC	8	6
Minamitorishima	153.9	24.3	1958	66		WOUDC	8	6
Mount Abu	72.7	24.6	1951	197	Brönnimann et al. 2003ab	WOUDC	12	6
Nashville	-86.6	36.3	1962	188		WOUDC	8	6
New Delhi	77.2	28.6	1955	284		WOUDC	12	6
New York	-73.9	40.9	1941	42	Brönnimann et al. 2003ab	internal	16	6
Olso	10.7	60.0	1946	55	Svendby et al. 2003	WOUDC	8	6
Oxford	-1.2	51.8	1925	403	Vogler et al. 2006	WOUDC	4	4
Perth	115.9	-31.9	1969	113		WOUDC	8	6
Potsdam	13.0	52.3	1926 (1957)	175		WOUDC	8	6
Quetta	66.5	30.1	1958	170		WOUDC	8	6
Rome	12.2	42.1	1954	285	Brönnimann et al. 2003ab	WOUDC	8	6
Sapporo	141.3	43.1	1958	249		WOUDC	8	6
Spitsbergen	15.0	78.0	1950	127	Vogler et al. 2005	WOUDC	8	6
Sterling	-77.5	39.0	1957	84		WOUDC	8	6
Table Mountain	-117.3	34.1	1926	14	Brönnimann 2005	internal	20	6
Table Mountain	-117.3	34.1	1928	13		internal	8	6
Taipeh	121.4	25.1	1965	76		WOUDC	8	6
Tallahassee	-84.4	30.4	1964	134		WOUDC	8	6
Tateno	140.1	36.1	1955	277	Brönnimann et al. 2003ab	internal/WOUDC	8	6
Toronto	-79.5	43.8	1960	220		WOUDC	8	6
Tromsoe	19.0	69.7	1935	344	Hansen and Svenoe 2005	WOUDC	4	4
Uppsala	17.6	59.9	1951	175		WOUDC	8	6
Varanasi	83.0	25.3	1957	170		WOUDC	8	6
Vladivostok	131.9	43.1	1973	66		WOUDC	8	6
ZiKaWei	121.4	31.2	1932	122	Brönnimann et al. 2003ab	WOUDC	16	6

Supplementary references

Baldwin, M. P., Gray, L. J., Dunkerton, T. J., Hamilton, K., Haynes, P. H., Randel, W. J., Holton, J. R., Alexander, M. J., Hirota, I., Horinouchi, T., Jones, D. B. A., Kinnersley, J. S., Marquardt, C., Sato K., Takahashi, M.: The Quasi-biennial oscillation, Reviews of Geophysics 39, 179-229, 2001.

Enfield, D. B., Mestas-Nunez, A. M., Trimble, P. J.: The Atlantic multidecadal oscillation and its relation to rainfall and river flows in the continental US, Geophys. Res. Lett., 28, 2077-2080, 2001.

Mantua, N. J., Hare, S. R., Zhang, Y., Wallace, J. M., Francis, R. C.: A Pacific interdecadal climate oscillation with impacts on salmon production, Bull. Am. Meterol. Soc., 78, 1069-1079, 1997.

Mégie, G., Chanin, M. L., Ehhalt, D., Fraser, P., Frederick, J. F., Gille, J. C., McCormick, M. P., Schoeberl. M.: Global trends. Chapter 2 in Scientific assessment of stratospheric ozone: 1989, Volume 1. World Meteorological Organization Global Ozone Research and Monitoring Project--Report no. 20. Geneva: World Meteorological Organization, 1989.

Tie, X. X., Brasseur, G.: The Response of Stratospheric Ozone to Volcanic-Eruptions – Sensitivity to Atmospheric Chlorine Loading, Geophys. Res. Lett., 22, 3035-3038, 1995.

WMO, Review of the Dobson spectrophotometer and its accuracy, Global Ozone Research and Monitoring Project, Report 13, WMO, Geneva, 1983.

WMO, World Meteorological Organization, Report of the WMO Meeting of Experts on Assessments of Performance Characteristics of Various Ozone Measuring Systems, Global Ozone Research and Monitoring Project, Report 9, WMO, Geneva, 1980.